ORIGINAL ARTICLE

WILEY

Ultrastructural identification of developing proximal tubules based on three-dimensional reconstruction

Jing Cong[1,2] | Shi-Jie Chang[3] | Jesper Skovhus Thomsen[4] | Arne Andreasen[4] | Xue Chen[1] | Jia Xing[1] | Jie Zhang[1] | Ling Gu[1] | Xiao-Yue Zhai[1] (ORCID)

[1] Department of Histology and Embryology, Basic Medical College, China Medical University, Shenyang, China

[2] Department of Histology and Embryology, Shenyang Medical College, Shenyang, China

[3] Department of Biomedical Engineering, College of Fundamental Science, China Medical University, Shenyang, China

[4] Department of Biomedicine–Anatomy, Aarhus University, Aarhus, Denmark

Correspondence
Xiao-Yue Zhai Professor, Department of Histology and Embryology, China Medical University, Shenyang, Liaoning, China.
Email: xyzhai@cmu.edu.cn

Abstract

Background: The cellular mechanisms involved in the development of proximal tubules are not only associated with morphogenesis in fetal life, but also with restoration of damaged tubules in adulthood. Knowledge about morphological features of cell differentiation and proliferation along the developing tubule is insufficient, which hinders identification of the cellular origin.

Objectives: This study aimed to investigate ultrastructures of the proximal tubule at different stages of nephrogenesis.

Methods: Electron microscopy was used and guided by computer-assisted tubular tracing to identify the cellular structures.

Results: Renal vesicles and S-shaped bodies revealed more proliferative features, such as densely-packed fusiform-shaped cells with numerous protein-producing organelles than membrane specializations typical for mature tubules. At the capillary-loop stage the proximal tubules demonstrated all characteristics of the mature tubules, but not as developed, including shorter but densely packed microvilli, fewer lateral processes with cell-cell contacts, lower basal membrane infoldings, and lower mitochondrial volume density. However, they exhibited an elaborated endocytic system above the nucleus, indicating a membrane transport is being established. Abundant free- and endoplasmic reticulum-adhered ribosomes and Golgi complexes reflected active protein synthesis for cell growth and proliferation. Interestingly, electron dense cells were occasionally intermixed with electron lucent cells characterized by various organelles in less cytosol and a larger nucleus with abundant euchromatin, which is a feature of active proliferation.

Conclusions: These ultrastructures indicate that the morphogenesis of the developing proximal tubule corresponds to the gradually established physiological activities. The two different cellular electron densities may suggest distinctive differentiation of the cells along the tubule.

KEYWORDS
developing kidney, proximal tubule, renal vesicle, S-shaped body, ultrastructure

1 | INTRODUCTION

The cellular mechanisms involved in the development of proximal tubules (PTs) are not only associated with morphogenesis but also with the restoration of damaged tubules in adulthood (Little & Kairath, 2017). The cellular origin for the regeneration is naturally linked to the PT cells at the different stages of differentiation during nephrogenesis.

Nephrogenesis is initiated by reciprocal signal induction between the ureteric bud (UB) tip and the metanephric mesenchyme. The latter then undergoes a so-called mesenchymal-to-epithelial transition, forming a renal vesicle (RV) composed of polarised epithelial cells (Pietilä & Vainio, 2014). The RV differentiates sequentially into a comma- and S-shaped bodies (SSB) with successive appearance of a lower (vascular) and an upper cleft. The SSB consists of two structurally different portions, a Bowman's capsule and a tubule anlages (Dørup, 1990). The tubule anlage includes histologically the upper (distal), middle and lower (proximal) limb, which will later become the distal convoluted tubule, Henle's loop and proximal convoluted tubule, respectively. The differentiation and transformation of RV and SSB require a series of precise proximal-distal gene patterning beginning as early as at the RV stage (Massa et al., 2013). During kidney development, plasma filtration does not start until capillary endothelial cells have invaded the vascular cleft of the SSB and the capillary loops have been formed (J. Zhang et al., 2017). At the same time, tubular reabsorption of the glomerular ultrafiltrate begins.

The PT derived from the proximal portion of RV and SSB undergoes quick growth and differentiation to become the longest mature segment of the renal tubule (Georgas et al., 2009). The PT is responsible for constitutive absorption of the glomerular ultrafiltrate, including water, electrolytes, small molecule proteins, amino acid, glucose and so forth, via a variety of transporters (Pohl et al., 2015; Sun et al., 2017). The transport is achieved with the assistance of membrane specialisations and an endocytic system in the cytoplasm. The membrane specialisations include a brush border consisting of densely packed microvilli on the luminal surface, lateral interdigitations and basal membrane infoldings. The endocytic system consists of coated pits and vesicles at the root of the microvilli, endosomes, apical dense tubules, and lysosomes (Eshbach & Weisz, 2017). The transportation is energy-driven, depending much on oxygen. The cells are therefore vulnerable to injuries like hypoxia, ischemia and nephrotoxins (Chevalier, 2016). Nevertheless, PT cells reveal a remarkable capacity to quickly restore or repair themselves following tubule damage (Shrestha et al., 2017). Genetically, there is a link between the kidney restoration after injury and kidney development (Fanni et al., 2015). However, information about cell structures and the biological activities during nephrogenesis is lacking, especially in mice.

The aim of the study was to extend our knowledge of the ultrastructure of the developing PT guided by computer-assisted tubular tracing. This may hopefully provide knowledge about the cellar proliferation during PT growth and restoration from tubular injuries in adulthood.

2 | MATERIALS AND METHODS

2.1 | Animals

Kidneys from embryonic (E) 17.5-day Kunming mice were studied. Animals were raised under standard specific-pathogen-free conditions. The animal experiments were performed in accordance with the code of Ethics of the World Medical Association (Declaration of Helsinki) and were approved by the Medical Ethics Committee of China Medical University (Shenyang, China).

2.2 | Renal tissue preparation and serial epoxy sectioning

The kidneys from three E17.5 mice were removed and fixed in 4% paraformaldehyde in 0.01 M phosphate-buffered saline (pH 7.4), post-fixed with 1% osmium tetroxide in 0.1 M sodium cacodylate buffer. The tissue blocks were dehydrated through graded concentrations of ethanol and acetol and then embedded in Epon 812 (TAAB, Aldermaston; P. Zhang et al., 2019). Finally, a total of 700 2.5-μm-thick serial epoxy sections were obtained for tubular tracing using a microtome (Reichert).

2.3 | Image acquirement and alignment

Images of the epoxy sections were obtained with a microscope (Nikon 90i) equipped with a Nikon DS digital camera. For each section, four partly overlapping digital images were recorded and combined into one 24-bit colour image using analySIS (version 3.2, Soft Imaging System).

All images were aligned by a custom-made computer program running on Linux (openSUSE 11.2, www.opensuse.org) as previously described in detail (Chang et al., 2015). The final image size was 2700 × 2000 pixels with an isotropic pixel size of 0.93 μm.

2.4 | Digital tracing and three-dimensional representation

The developing nephron was traced using custom-made software on the Linux system as previously described in detail (J. Zhang et al., 2017). Tubular path distances were derived from the tracing data as previously described (Zhai et al., 2006). The tracing started at the urinary pole of the renal corpuscle at the capillary loop stage and ended at the transition between the cuboidal PT epithelium and the squamous epithelium of the descending thin limb of Henle's loop.
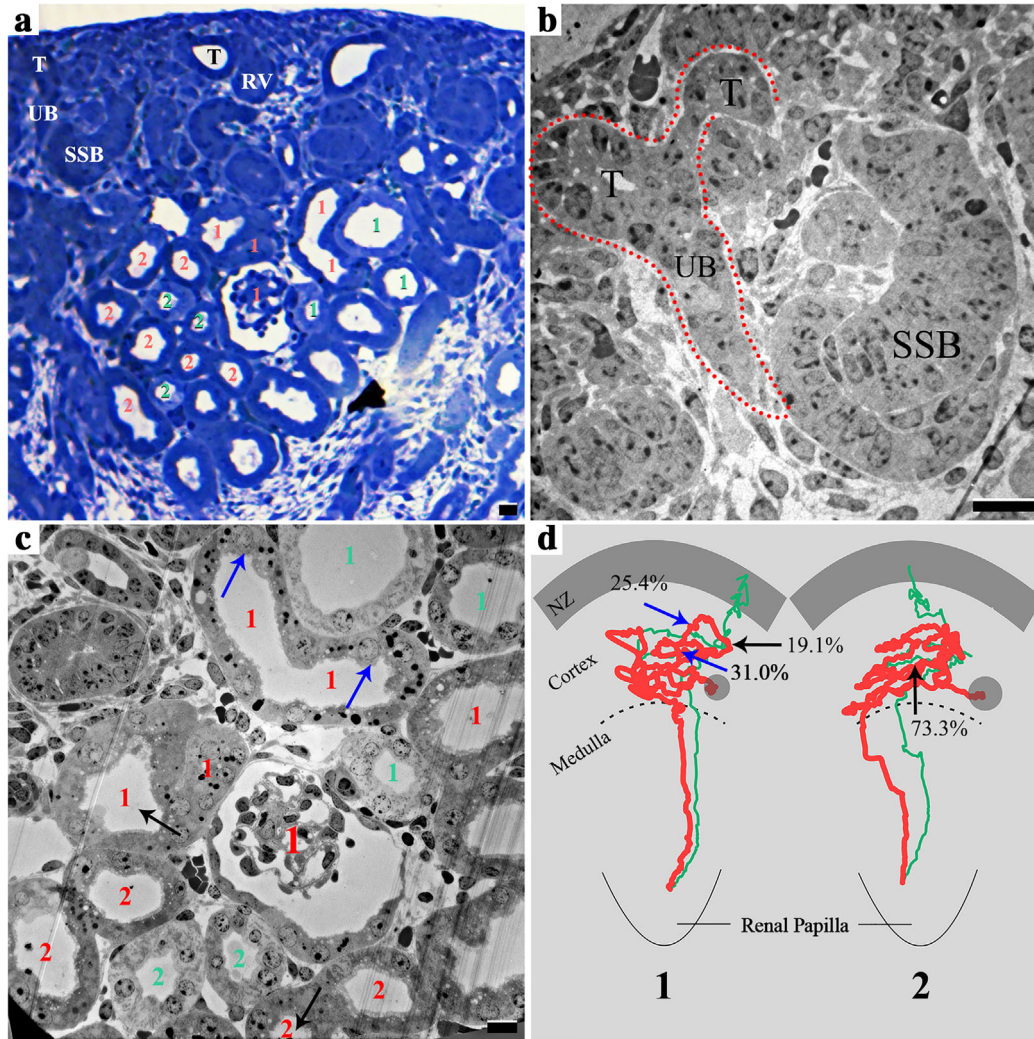
FIGURE 1 Light and electron micrographs derived from the same serial section from an E17.5 mouse kidney. (a) The light micrograph contains various nephrogenic structures, including renal vesicle (RV) connecting to a ureteric bud (UB) tip (T), an S-shaped body (SSB), and traced tubules at the capillary loop stage. The numbers in red and green correspond to the spatially traced tubules in Figure 1d. (b) The electron micrograph showing the SSB in Figure 1a. According to the tubular tracing, the upper end of the tubule anlage connects to the UB tip (T) shown as a red dotted line. (c) The electron micrograph showing the traced tubules adjacent to one of the traced nephron glomeruli, corresponding to a smaller region in Figure 1a. The blue arrows point to two electron-lucent cells located 25.4% and 31.0% along the PT lengths determined by 3-D tracing seen in Figure 1d. (d) 3-D representations of two traced nephrons at the capillary loop stage. The nephron is composed of a renal corpuscle (grey sphere), a proximal convoluted segment continuing into the descending limb (red line) and the ascending limb continuous with the distal convoluted tubule (green line). Bars: 100 μm (a), 10 μm (b, c)

2.5 | Electron microscopy and measurement of volume density of mitochondrion

Based on the three-dimensional (3-D) tracing, epoxy sections containing the nephrogenic zone, cortex and medulla were selected. These sections were re-embedded in Epon 812 and cut into 50-nm-thick ultrathin sections for ultrastructural analysis. Electron micrographs were obtained using an electron microscope (Hitachi, H-7650 and JM-1400 flash) at magnifications from ×1000 to ×25,000.

Three electron micrographs of each PT cross-section were taken randomly at a well-defined length from the glomerulus for measuring the thickness of the basement membrane (×15,000) and the height of the microvilli (×8000). The volume densities of mitochondria were

determined using point-counting (Baddeley & Jensen, 2004; Howard & Reed, 2005) in Photoshop CS6:

$$V_V = \sum Pi \Big/ \sum Pc, \qquad (1)$$

where $\sum Pi$ is the sum of points hitting on mitochondria and $\sum Pc$ is the sum of points hitting on the reference space (cytoplasm).

3 | RESULTS

Nephrons at different developing stages were located in inverse sequence to nephrogenesis throughout the cortex of E17.5 kidneys (Figure 1). Newly formed nephrons, RVs and SSBs were located around
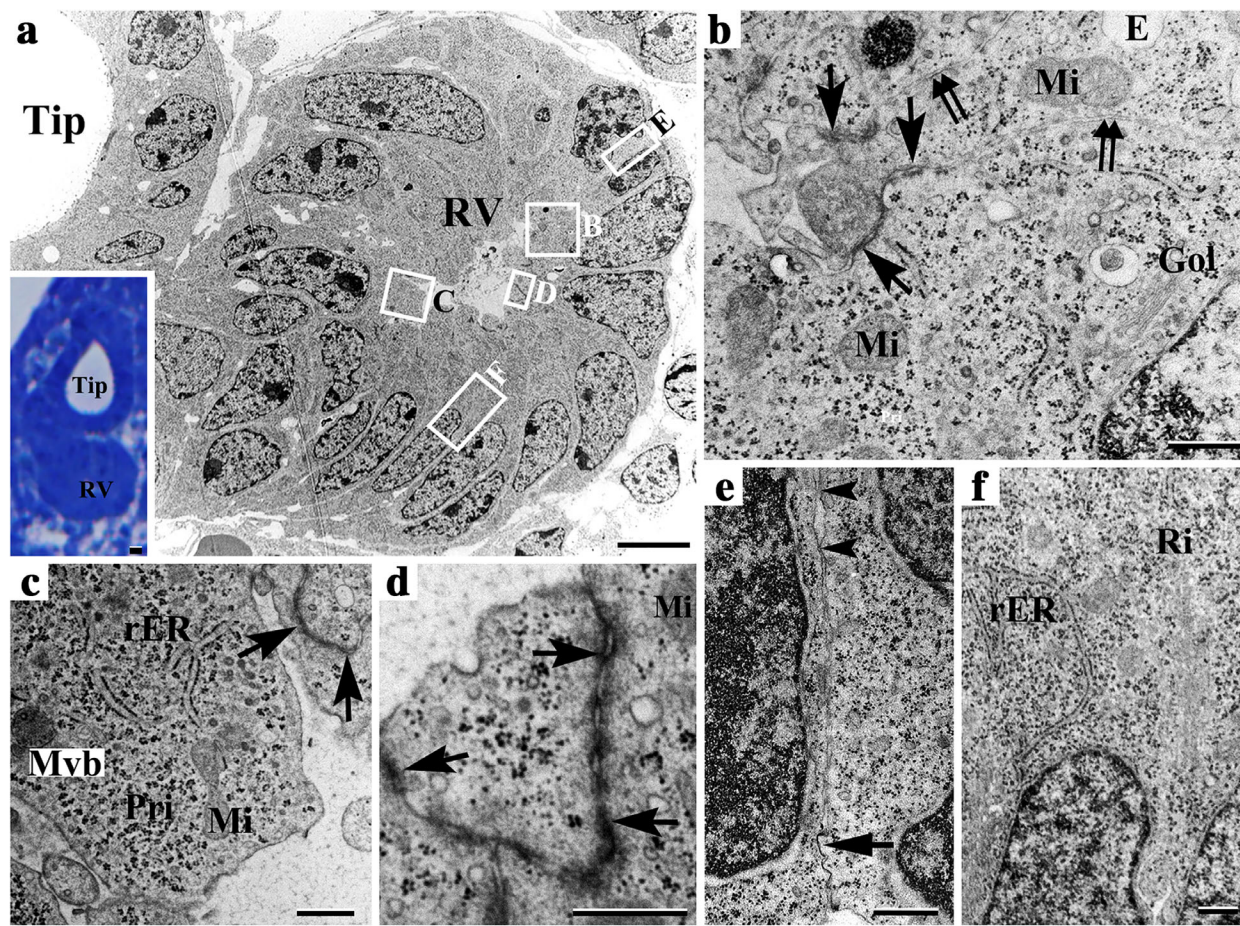
FIGURE 2 Electron micrographs showing an RV connecting to a UB tip. RV, renal vesicle; Tip, ureteric bud tip; Mi, mitochondria; rER, rough endoplasmic reticulum; Pri, polyribosome; Ri, ribosome; E, endosome; Gol, Golgi complex; CP, coated pit; CV, coated vesicle; Mvb, multivesicular body. (a) An RV connecting to a Tip shown at lower magnification in inlet. (b) The region corresponding to the white frame 'b' in Figure 2a, showing the apical part of a cell from the proximal end of the RV. There are scattered Mi, rER and Gol in the cytoplasm. Small vesicles are seen budding from Gol. The lateral membranes of neighbouring cells are close and form a junctional complex (black arrows) at the luminal top. Beneath the junctional complexes, the lateral membranes are separated by a narrow intercellular space (double black arrow). (c) The region corresponding to the white frame 'c' in Figure 2a, showing the apical part of a cell from the distal end of the RV. There are abundant Pri, interspersed with Mi, RER and Mvb. Black arrows indicate the junctional complex. (d) Image at high magnification corresponding to the white frame 'd' in Figure 2a, showing the invaginated CP and CV at the free surface of the cell, as well as junctional complexes sealing the apical intercellular space (black arrows). (e) The region corresponding to the white frame 'e' in Figure 2a, showing the straight and narrow intercellular space. At some point, the two opposing plasma membranes are fused into an electron-dense membrane (black arrow), or form bead-like contacts (black arrow heads). (f) The region corresponding to the white frame 'f' in Figure 2a, showing a part of the two neighbouring cells. The boundary of the two cells is blurred compared to those in Figure 2b (arrows) and Figure 2e (arrowheads). Bars: 5 μm (a) and 0.5 μm (b–f)

the transition of the nephrogenic zone and superficial cortex, together with the terminal tips of UB (Figures 1a,b). According to the tubular tracing, relatively mature tubules and glomeruli were identified in the middle to the juxta-medullary cortex (Figures 1c,d). In general, the cells in the RV and SSB did not show membrane specialisations and cytoplasmic features typical for any of the mature tubule segments until the capillary loop stage, where the PT demonstrated ultrastructural features similar to those of mature PT.

3.1 | RV and SSB

According to the proximal-distal gene patterning (Little et al., 2010), the distal and proximal portion of the RV will differentiate in different

directions. The distal end of the RV connected to the tip ampulla of the UB at the nephrogenic zone beneath the renal capsule, while the proximal end of the RV, which will differentiate into the glomerulus, was farthest from the UB tip.

The cells and their nuclei in the distal and proximal ends were highly irregular in shape, and the middle part of the RV consisted of a layer of densely packed fusiform cells with fusiformed nuclei (Figure 2a).

These cells encircled a very narrow lumen, and a few short and blunt cytoplasmic processes were located at the luminal surface of the cells (Figure 2b). The lateral intercellular space was narrow and straight and was sealed at the luminal top by well-developed junctional complexes composed of zonula occludens and zonula adherens (Figures 2b–d). At
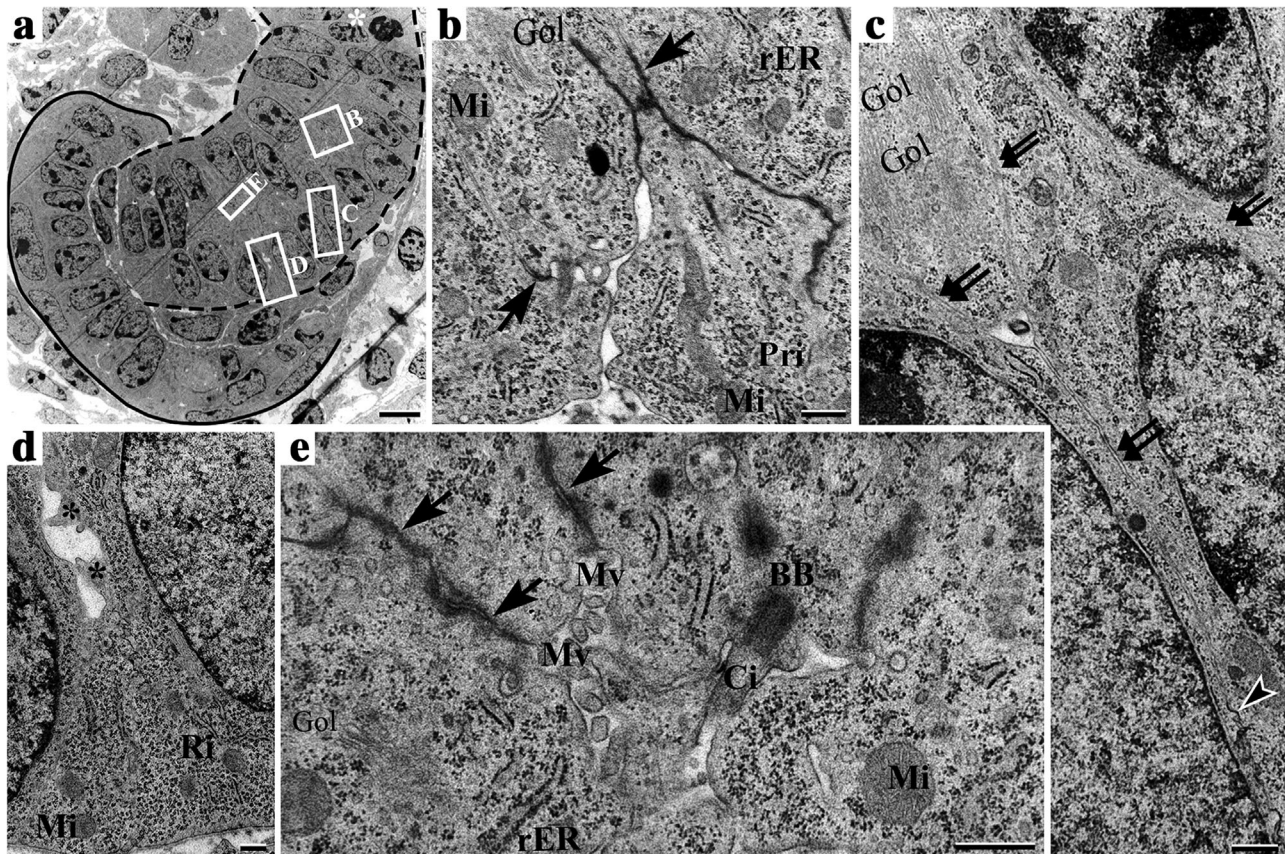
FIGURE 3 Electron micrographs showing an SSB. Mv, microvilli; Ri, ribosomes; Mi, mitochondrion; Gol, Golgi complex; Pri, polyribosome; rER, rough endoplasmic reticulum; BB, basal body; Ci, cilium. (a) An SSB composed of a Bowman's capsule anlage (lower left) and a renal tubule anlage (dashed line). White asterisk: distal limb. (b) Apical part of the epithelial cells in the renal tubule anlage. The apical part of the neighbouring cell membranes forms junctional complex (black arrows). Cytoplasm is filled with abundant Pri, Gol, rER and Mi. (c) The lateral region of two neighbouring cells. Intercellular space is narrow and straight (double black arrows) with focal fusion of lateral opposing membranes (black arrowhead). (d) The basal-lateral part of the epithelial cells in the renal tubule anlage. A relatively broad intercellular space with a few bulky cellular processes is seen (black asterisks). (e) The apical surface of the epithelial cells. A few tiny microvilli protrude into the lumen. A cilium can occasionally be seen arising from the basal body. Junctional complex between two adjacent cells (black arrows). Bars: 5 μm (a) and 0.5 μm (b–e)

times, the two opposing plasma membranes were seen to form bead-like contacts or to fuse into an electron-dense membrane (Figure 2e). Occasionally, a blurred boundary was seen between neighbouring cells, especially at the main body of the RV (Figure 2f). The basal membrane was flush against a thin basal lamina, without plasma membrane infoldings. Inside the cells, the apical endocytic system, such as apical dense tubules or coated pits and vesicles were often seen, while endosomes were rarely seen (Figure 2d). However, polyribosomes were extensively present throughout the cytoplasm, interspersed with mitochondria and rough endoplasmic reticulum (rER). Golgi complexes were often seen close to the nucleus; however, they were not well developed (Figure 2b).

The newly formed SSB consisted of two anlages, a Bowman's capsule and tubular anlages arising from the capsule anlage and connecting with the terminal UB tip (Figure 3a). The Bowman's capsule anlage consisted of two layers of epithelia with an almost invisible lumen in between, an outer layer of flattened cells and an inner layer of low columnar cells (Figure 3a). The tubule anlage consisted of a simple layer

of densely packed fusiform cells, and the lumen was almost invisible. In addition, between the two anlages, the capillary loops were not formed. We further examined the cells constituting the tubular anlage. The cell membrane surfaces and cytoplasmic organelles of the cells were similar to those in the main body of the RV (Figures 3b–e). Occasionally, a blurred boundary was seen between the neighbouring cells. Sometimes, the two opposing plasma membranes fused into an electron-dense membrane (Figure 3c). The basement membrane had a thin basal lamina. Compared to the RV, the SSB was equipped with few microvilli and occasionally a cilium on the luminal surface of the cells in the proximal limb (Figure 3e). No lateral membrane processes and basal membrane infoldings were found.

3.2 | at the capillary loop stage

The 3-D tubular tracing revealed that the PT from the capillary loop stage nephrons took a similar path to mature PT but were much shorter
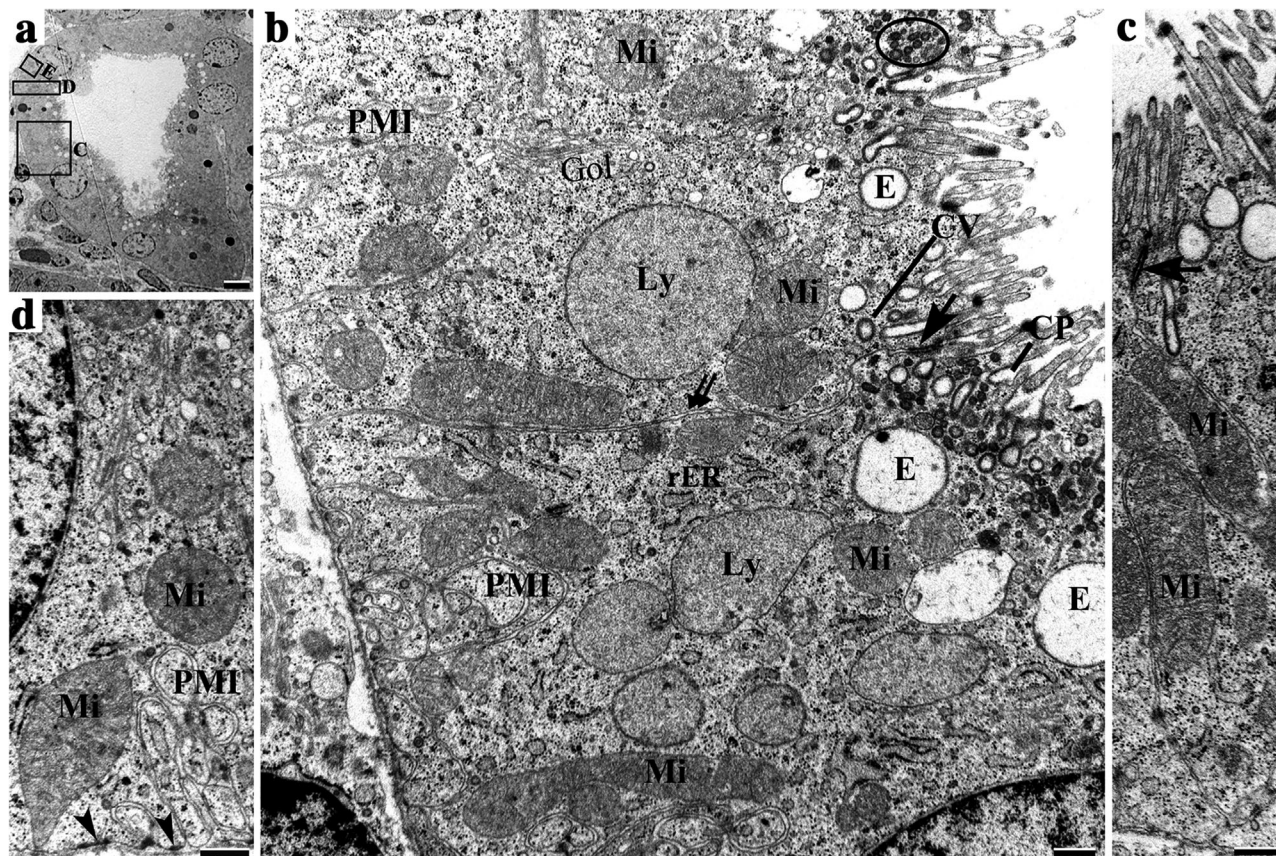
FIGURE 4 Electron micrographs showing the initial part of a proximal tubule (PT) at the capillary loop stage. Mi, mitochondrion; rER, rough endoplasmic reticulum; Pri, polyribosome; Ri, ribosome; E, endosome; Ly, lysosome; Gol, Golgi complex; CP, coated pit; CV, coated vesicle; Mvb, multivesicular body; PMI, plasma membrane infolding. (a) A tubular cross-section at 19.1% of the whole length of the PT from the glomerulus. (b) The cell is characterised by densely packed microvilli, a developed endocytotic apparatus including coated pits, coated vesicles, endosomes and lysosomes at the apical cytoplasm, and short plasma membrane infoldings at the basal cytoplasm. Intercellular space (double black arrow), dense apical tubules (black ellipse), junctional complex (black arrow). (c) Intercellular space of adjacent tubular epithelial cells. The lateral processes contain rod-like mitochondria interdigitating with lateral processes of the neighbouring cell. Cell contacts (black arrow). (d) The basal part of the epithelial cell. The plasma membrane infoldings are tiny and short. Hemidesmosomes (black arrowheads). Bars: 5 μm (a) and 0.5 μm (b–d)

(Figure 1d). The PT cells were examined at well-defined distances from their own glomeruli. The ultrastructure of cell membrane specialisations, endocytic system and cellular organelles did not vary much from the initial part to the end (from 6.1% to 95% of the total PT length; Figures 1c,d, 4 and 5).

Apical surface. The average height of the densely packed microvilli (1.39 μm) was nearly half of that seen in adult kidneys (2.76 μm; Zhai et al., 2003), and the microvilli height did not change much from the proximal to the distal part of the PT (Figures 4a–d).

Lateral surface. The lateral cytoplasmic membranes of adjacent cells were parallel and separated by a narrow and straight intercellular space. Junctional complexes including electron-dense zonula occludens and zonula adherens were observed at each apical intercellular space. Desmosomes were often present in the centre of the intercellular space. The lateral processes varied in size and shape from a local bump to a finger-like invagination, mainly located in the mid to lower part of the intercellular space (Figures 4a–d).

Basal surface. The basement membrane was 52–87 nm thick. Hemidesmosomes were occasionally observed between the basal surface of the epithelial cells and the basal membrane. Small and short invaginations, that is, plasma membrane infoldings, occupied the basal part of the cytoplasm together with rod-like mitochondria, while higher invaginations were rarely seen (Figures 4b,d and 5b,c).

Endocytic system. The immature PT contained a relatively well developed endocytic system including coated pits and vesicles at the base of the microvilli, apical dense tubules and endosomes distributed in the area above the nuclei. The lysosomes varied considerably in size and inclusion. The number of electron-dense lysosomes decreased from the proximal to the distal PT. Many multivesicular bodies were found in the distal part of the PT.

Mitochondria. Most mitochondria seemed to be randomly oriented. Long rod-shaped or oval mitochondria were found nearby or inside the basolateral processes. In addition, ring-, U- and dumbbell-shaped mitochondria were present (Figures 4c and 5b). The volume density of the
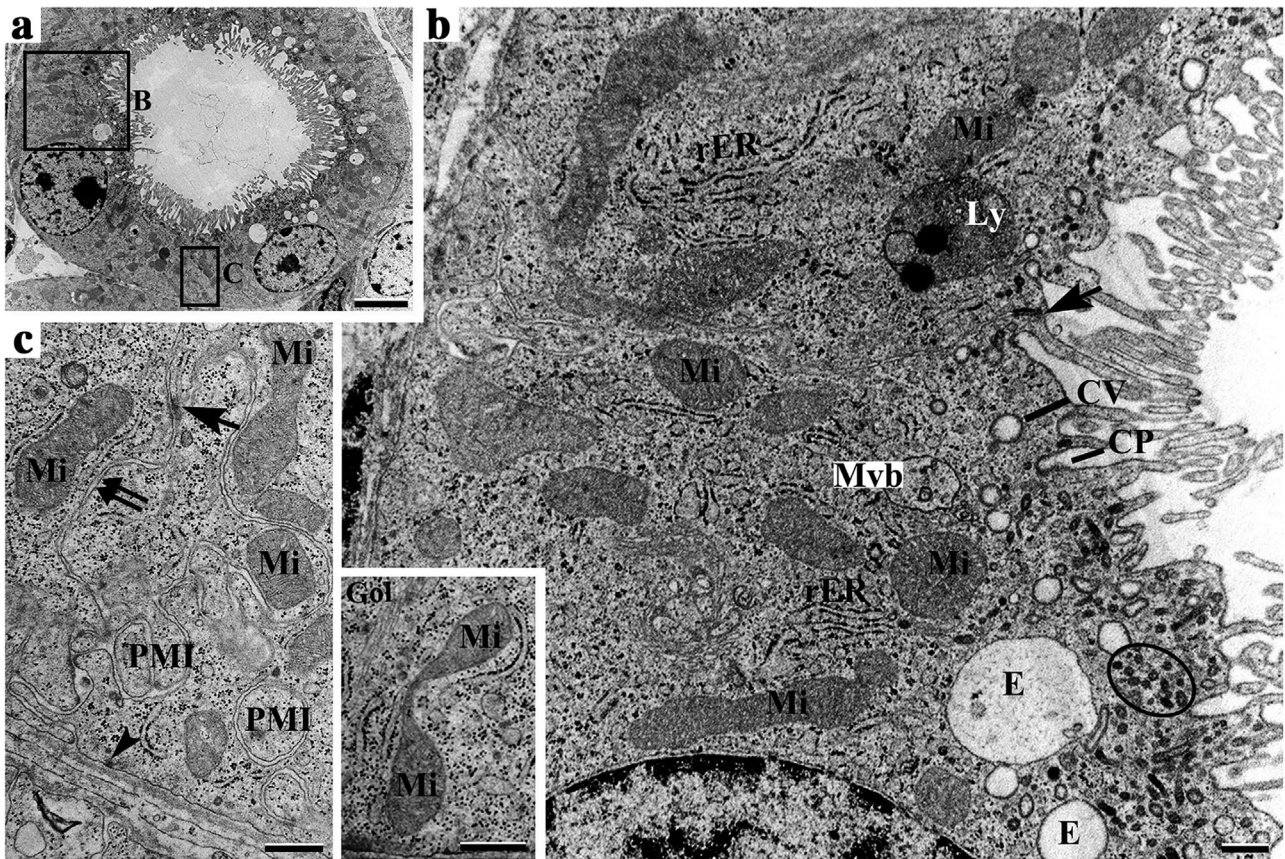
FIGURE 5 Electron micrographs showing the late part of the PT at the capillary loop stage. CP, coated pit; CV, coated vesicles; Mi, mitochondrion; Ly, lysosome; rER, rough endoplasmic reticulum; Gol, Golgi complex; Mvb, multivesicular body; E, endosomes. (a) A tubular cross-section at 73.3% of the whole length of the PT from the glomerulus. (b) The endosome including dense apical tubules (black ellipse), coated pits, coated vesicles, and endosomes at the apical part, as well as organelles in the main body of the cell, including dumbbell-shaped mitochondria (inlet), rER and Golgi complex parallel to the rod-shaped mitochondria, electron-dense lysosomes. (c) The lateral-basal part of the epithelial cell. The basolateral interdigitations are further developed, compared to the early part of the epithelial cells shown in Figure 4b . Fewer and smaller plasma membrane infoldings than in Figure 4b. In addition, cell contacts (black arrow) and hemidesmosome (black arrowhead) are observed along the basolateral membrane. Intercellular space (double black arrow). Bars: 5 μm (a) and 0.5 μm (b–c)

mitochondria was 10.7%–16.8% (compared to an average volume density of 44% in an adult kidney).

Free ribosomes and rER. Free- and rER-adhered ribosomes were abundant throughout the cytoplasm, interspersed with mitochondria. Thin, line-shaped rER, similar to those in RV and SSB, was often seen parallel to the lateral boundary of the cells. Especially in the late PT, 2069 μm and 2573 μm distant from their glomeruli (69.0% and 76.2% of the whole length of the PT), the rER was thinner and longer (Figure 5) than in the initial PT (Figure 4).

3.3 | Electron lucent (light) cells along capillary loop stage nephron

At the capillary loop stage, electron-lucent (light) cells were often found in the second quarter (25%–31% of the total PT length). These 'light' cells were randomly interspersed with the majority of the PT

cells that was relatively electron-dense (dark). The 'light' cells had less cytosol and a larger and round nucleus with abundant euchromatin (Figures 6a–d). In addition, the 'light' cells contained fewer mitochondria, rER, Golgi complexes, lysosomes and ribosomes than the neighbouring dark cells. Furthermore, the membrane specialisations of the 'light' cells were poorly developed, compared to the neighbouring dark cells, that is, the microvilli were sparse, lateral processes were shorter and fewer and the basal membrane infoldings were short or absent (Figures 6b–f).

4 | DISCUSSION

The cellular origin of PT regeneration is debated but is believed to be related to the cellular proliferation and differentiation along the PT during nephrogenesis.

The PT is genetically derived from the middle portion of the RV and the lower limb of the tubule anlage of SSB. In the present study, this
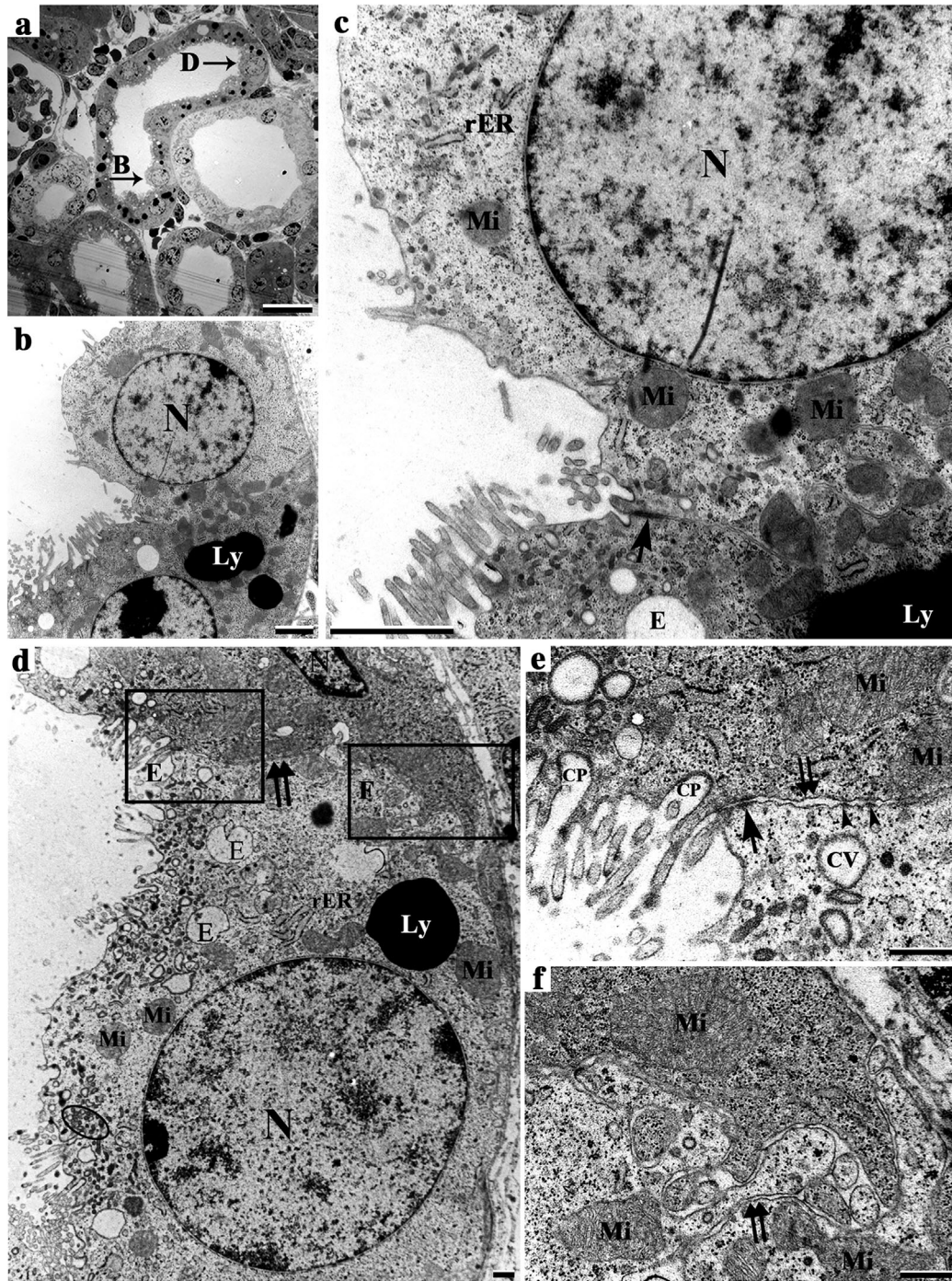
FIGURE 6 Electron micrographs showing electron-lucent (light) cells neighbouring with electron-dense (dark) cells along PT at the capillary loop stage. N, nucleus; Mi, mitochondrion; Ri, ribosome; rER, rough endoplasmic reticulum; Ly, lysosome. (a) The 'light' cells (arrows) at lower magnification along the PTs. (b) One 'light' cell and a part of a 'dark' cell (lower) at 31.1% of the whole length of the PT, distant from glomerulus. (c) The 'light' cell corresponding to Figure 6b has a larger and round nucleus with abundant euchromatin, fewer organelles including mitochondria, ribosomes, rER, and lysosomes, and less basal membrane infoldings, in addition to less cytosol substance, compared to the 'dark' cell. The microvilli are shorter and more loosely packed in the 'light' cell. (d) The other 'light' cell and a part of a 'dark' cell (upper) at 25.4% of the whole length of the PT, distant from the glomerulus. The endocytic system including dense apical tubules (black ellipse), coated pits, coated vesicles and endosomes at apical cytoplasm are scattered in the apical cytoplasm of the 'light' cell. The intercellular space (double black arrows) is straight and narrow. (e) The apical-lateral part of a 'light' and a 'dark' cell. Coated pits, coated vesicles, junctional complexes (black arrow) and a few zonula adherens (black arrowheads) along the intercellular space (double black arrows). (f) Basal lateral part a 'light' and a 'dark' cell with a few interdigitating processes with mitochondria. Bars: 20 μm (a), 2 μm (b, c) and 0.5 μm (d–f)

was reflected by the microstructural features of the epithelial cells in the RV and SSB, such as densely packed fusiform cells with abundant polyribosomes and rER and numerous Golgi complexes throughout the cytoplasm. The developing PT quickly proliferated–probably by amitosis in the RV and SSB. This is also supported by the observation that the apparatus for the mitotic division was sparse and that the dividing nuclei were rarely seen in RV and SSB. In contrast to proliferation, the features for cell differentiation in the RV and SSB were not that prominent. However, the genetically patterned domains of both RV and SSB revealed specific characteristics, reflecting distinct differentiation in different cell groups. First, the distal and proximal ends of the RV were both composed of densely packed cuboidal cells with highly irregular-shaped nuclei. The distal end of the RV connected to the UB tip (P. Zhang et al., 2019), while the proximal end proceeded into a Bowman's capsule anlage of the SSB. The newly formed SSB had a collapsed capsule and tubule lumen indicating that a real filtration had not yet been established. This is also supported by the lack of histological and ultrastructural features for absorptive function along the tubule anlage of the SSB.

No matter how packed the epithelial cells were, the junctional complexes were never absent and were well developed, which is a hallmark of polarised epithelium.

As the capillary loops develop, the tubule anlage of the SSB quickly grows and differentiates, thereby forming the different segments of the renal tubule with filtering function at the capillary loop stage. In the present study, we showed that the cells at all examined PT points exhibited characteristics similar to those of mature PT, including membrane specialisations and localisation of the endocytic system above the nuclei. However, the volume density of the mitochondria was much lower than that of adult kidneys (Zhai et al., 2006). The observed polymorphic mitochondria might imply that the cells were mito-biogenetically or mito-dynamically active (Baker et al., 2019). Furthermore, the PT cells at the capillary loop stage also exhibited morphological features related to protein synthesis and endocytosis, meaning that the PT is equipped with organelles for proliferation and differentiation as well as for absorption of the ultrafiltrate.

The fact that the PT can restore after acute damage, has aroused interest in the cellular basis for tubular regeneration (Yoshida & Honma, 2014). Some studies have shown an overlap in gene expression in the signalling pathways for kidney development and the instant response to renal injury (Duffield & Humphreys, 2011; Little & Kairath, 2017). Furthermore, studies have reported that the number of CD24-positive, CD133-positive and vimentin-positive cells scattered throughout the PT in normal human kidneys increases after acute tubular injury (Lindgren et al., 2011). CD24-positive cells contain less cytoplasm and fewer mitochondria and have no brush border in contrast to the adjacent 'normal' PT cells (Smeets et al., 2013). The 'light' cells we found in the present study had features similar to the above described CD24-positive cells. These 'light' cells were intermixed with the neighbouring electron-dense cells that form the majority of the PT cells at the capillary loop stage. The source of the regenerative cells may be aroused quiescent progenitor cells (Angelotti et al., 2012) or dedifferentiated surviving mature tubular cells (Lombardi et al., 2016). In order to clarify whether the 'light' cells found in the present study are related to the progenitor cells or the dedifferentiated cells, further investigation is needed.

In summary, the present study provided a detailed description of the ultrastructure of the cells at RV, SSB and capillary loop stage PT. The structural features reflected different biological activities at different nephrogenic stages, for example, cell proliferation dominantly in the earlier stages and differentiation in the later stages. In addition, the present study described a population of 'light' cells, which had structural features similar to the potential stem cells (CD24-positive cells), suggesting a candidate cell for tubule regeneration.

ETHICS STATEMENT

The authors confirm that the ethical policies of the journal, as noted on the journal's author guidelines page, have been adhered to and the appropriate ethical review committee approval has been received. The US National Research Council's guidelines for the Care and Use of Laboratory Animals were followed.

AUTHOR CONTRIBUTIONS

Jing Cong performed the experiments and wrote the manuscript draft; Shi-Jie Chang wrote the computer program for aligning the digital images; Jesper Skovhus Thomsen and Arne Andreasen composed the computer programs for image alignment and tubular tracing; edited the manuscript with discussion; Xue Chen prepared the renal tissue for taking electron micrographs; Jia Xing took the electron micrographs of renal vesicle; Jie Zhang analysed the data and edited the graphs of digital tracing; Ling Gu analysed the data from 3-D reconstruction; Xiao-Yue Zhai designed and supervised the experiments and edited the final manuscript.

CONFLICT OF INTEREST

The authors declare that they have no conflicts of interests.

DATA AVAILABILITY STATEMENT

The data that support the findings of this study are available from the corresponding author upon request.

PEER REVIEW

The peer review history for this article is available at https://publons.com/publon/10.1002/vms3.558.

ORCID

Xiao-Yue Zhai https://orcid.org/0000-0001-5907-8257

REFERENCES

Angelotti, M. L., Ronconi, E., Ballerini, L., Peired, A., Mazzinghi, B., Sagrinati, C., Parente, E., Gacci, M., Carini, M., Rotondi, M., Fogo, A. B., Lazzeri, E., Lasagni, L., & Romagnani, P. (2012). Characterization of renal progenitors committed toward tubular lineage and their regenerative potential in renal tubular injury. *Stem Cells*, 30(8), 1714–1725. https://doi.org/10.1002/stem.1130

Baddeley, A., & Jensen, E. B. (2004). *Stereology for statisticians*. Chapman & Hall/CRC. https://doi.org/10.1201/9780203496817

Baker, N., Patel, J., & Khacho, M. (2019). Linking mitochondrial dynamics, cristae remodeling and supercomplex formation: How mitochondrial structure can regulate bioenergetics. *Mitochondrion*, 49, 259–268. https://doi.org/10.1016/j.mito.2019.06.003</bib>

Chang, S. J., Li, S., Andreasen, A., Sha, X. Z., & Zhai, X. Y. (2015). A reference-free method for brightness compensation and contrast enhancement of micrographs of serial sections. *PloS One*, 10(5), e0127855. https://doi.org/10.1371/journal.pone.0127855

Chevalier, R. L. (2016). The proximal tubule is the primary target of injury and progression of kidney disease: Role of the glomerulotubular junction. *American Journal of Physiology: Renal Physiology*, 311(1), F145–F161. https://doi.org/10.1152/ajprenal.00164.2016

Dørup, J. (1990). Ultrastructure of the distal nephron. An analysis of structure-function relationships in distal nephron segments of the kidney. *Danish Medical Bulletin*, 37, 502–506.

Duffield, J. S., & Humphreys, B. D. (2011). Origin of new cells in the adult kidney: Results from genetic labeling techniques. *Kidney International*, 79(5), 494–501. https://doi.org/10.1038/ki.2010.338

Eshbach, M. L., & Weisz, O. A. (2017). Receptor-Mediated Endocytosis in the Proximal Tubule. *Annual Review of Physiology*, 79, 425–448. https://doi.org/10.1146/annurev-physiol-022516-034234

Fanni, D., Sanna, A., Gerosa, C., Puddu, M., Faa, G., & Fanos, V. (2015). Each niche has an actor: Multiple stem cell niches in the preterm kidney. *Italian Journal of Pediatrics*, 41, 78. https://doi.org/10.1186/s13052-015-0187-6

Georgas, K., Rumballe, B., Valerius, M. T., Chiu, H. S., Thiagarajan, R. D., Lesieur, E., Aronow, B. J., Brunskill, E. W., Combes, A. N., Tang, D., Taylor, D., Grimmond, S. M., Potter, S. S., McMahon, A. P., & Little, M. H. (2009). Analysis of early nephron patterning reveals a role for distal RV proliferation in fusion to the ureteric tip via a cap mesenchyme-derived connecting segment. *Developmental Biology*, 332(2), 273–286. https://doi.org/10.1016/j.ydbio.2009.05.578

Howard, C. V., & Reed, M. G. (2005). *Unbiased stereology: Three-dimensional measurement in microscopy*. Garland Science/BIOS Scientific.

Lindgren, D., Bostrom, A. K., Nilsson, K., Hansson, J., Sjolund, J., Moller, C., Jirström, K., Nilsson, E., Landberg, G., Axelson, H., & Johansson, M. E. (2011). Isolation and characterization of progenitor-like cells from human renal proximal tubules. *American Journal of Pathology*, 178(2), 828–837. https://doi.org/10.1016/j.ajpath.2010.10.026

Little, M., Georgas, K., Pennisi, D., & Wilkinson, L. (2010). Kidney development: Two tales of tubulogenesis. *Current Topics in Developmental Biology*, 90, 193–229. https://doi.org/10.1016/s0070-2153(10)90005-7

Little, M. H., & Kairath, P. (2017). Does renal repair recapitulate kidney development? *Journal of the American Society of Nephrology*, 28(1), 34–46. https://doi.org/10.1681/ASN.2016070748

Lombardi, D., Becherucci, F., & Romagnani, P. (2016). How much can the tubule regenerate and who does it? An open question. *Nephrology, Dialysis, Transplantation*, 31(8), 1243–1250. https://doi.org/10.1093/ndt/gfv262

Massa, F., Garbay, S., Bouvier, R., Sugitani, Y., Noda, T., Gubler, M. C., Heidet, L., Pontoglio, M., & Fischer, E. (2013). Hepatocyte nuclear factor 1β controls nephron tubular development. *Development*, 140(4), 886–896. https://doi.org/10.1242/dev.086546

Pietilä, I., & Vainio, S. J. (2014). Kidney development: An overview. *Nephron Experimental Nephrology*, 126(2), 40–44. https://doi.org/10.1159/000360659

Pohl, M., Shan, Q., Petsch, T., Styp-Rekowska, B., Matthey, P., Bleich, M., Bachmann, S., & Theilig, F. (2015). Short-term functional adaptation of aquaporin-1 surface expression in the proximal tubule, a component of glomerulotubular balance. *Journal of the American Society of Nephrology*, 26(6), 1269–1278. https://doi.org/10.1681/ASN.2014020148

Shrestha, S., Somji, S., Sens, D. A., Slusser-Nore, A., Patel, D. H., Savage, E., & Garrett, S. H. (2017). Human renal tubular cells contain CD24/CD133 progenitor cell populations: Implications for tubular regeneration after toxicant induced damage using cadmium as a model. *Toxicology and Applied Pharmacology*, 331(3), 116–129. https://doi.org/10.1016/j.taap.2017.05.038

Smeets, B., Boor, P., Dijkman, H., Sharma, S. V., Jirak, P., Mooren, F., Berger, K., Bornemann, J., Gelman, I. H., Floege, J., van der Vlag, J., Wetzels, J. F., & Moeller, M. J. (2013). Proximal tubular cells contain a phenotypically distinct, scattered cell population involved in tubular regeneration. *Journal of Pathology*, 229(5), 645–659. https://doi.org/10.1002/path.4125

Sun, J., Hultenby, K., Axelsson, J., Nordstrom, J., He, B., Wernerson, A., & Lindstrom, K. (2017). Proximal tubular expression patterns of megalin and cubilin in proteinuric nephropathies. *Kidney International Reports*, 2(4), 721–732. https://doi.org/10.1016/j.ekir.2017.02.012

Yoshida, M., & Honma, S. (2014). Regeneration of injured renal tubules. *Journal of Pharmacological Sciences*, 124(2), 117–122. https://doi.org/10.1254/jphs.13R12CP

Zhai, X. Y., Birn, H., Jensen, K. B., S, J. T., Andreasen, A., & Christensen, E. I. (2003). Digital three-dimensional reconstruction and ultrastructure of the mouse proximal tubule. *Journal of the American Society of Nephrology*, 14(3), 611–619. https://doi.org/10.1097/01.asn.0000051725.00406.0c

Zhai, X. Y., Thomsen, J. S., Birn, H., Kristoffersen, I. B., Andreasen, A., & Christensen, E. I. (2006). Three-dimensional reconstruction of the mouse nephron. *Journal of the American Society of Nephrology*, 17(1), 77–88. https://doi.org/10.1681/ASN.2005080796

Zhang, J., Cong, J., Yang, J., Thomsen, J. S., Andreasen, A., Chang, S.-J., Wang, K. Y., Gu, L., & Zhai, X.-Y. (2017). Morphologic and morphometric study on microvasculature of developing mouse kidneys. *American Journal of Physiology: Renal Physiology*, 315(4), F852–860. https://doi.org/10.1152/ajprenal.00615.2017

Zhang, P., Gu, L., Cong, J., Zhang, J., Thomsen, J. S., Andreasen, A., Chang, S. J., Deng, S. Q., Xing, J., & Zhai, X. Y. (2019). Morphology of the initial nephron-collecting duct connection in mice using computerized 3D tracing and electron microscopy. *Biochemical and Biophysical Research Communications*, 509(1), 114–118. https://doi.org/10.1016/j.bbrc.2018.12.079